Mechanics of Materials 140 (2020) 103244

Contents lists available at ScienceDirect

Mechanics of Materials

journal homepage: www.elsevier.com/locate/mechmat

Research paper

Micromechanical behavior of ultraviolet-exposed polyurea

Atif Mohammed Shaik, Nha Uyen Huynh, George Youssef*

Experimental Mechanics Laboratory, Mechanical Engineering Department, San Diego State University, 5500 Campanile Drive, San Diego, CA 92182 USA

A B S T R A C T

The present study focuses on the microstructural characterization of polyurea after extended UV exposure using a mechanics-based, atomic force microscope (AFM) investigation. Extended exposure to UV radiation resulted in photo-degradation with subsequent photo-oxidation reactions causing an increase in the surface roughness associated with crack nucleation. The crack opening and length were found to increase considerably with the rise in UV exposure duration. The crack growth was modeled using linear elastic fracture mechanics (LEFM) since the mechanical properties of the surface degraded layer were found to be within the limits of applicability of the theory. Force-distance measurements performed on the surface of the samples revealed a significant increase in the local modulus after 4.5 weeks of exposure. The local modulus was found to reach a steady limit after 7.5 weeks of UV radiation. The adhesive tip-sample forces resolved from the AFM force-displacement measurements indicated a drastic decrease after 3 weeks of exposure due to embrittlement of photo-oxidized exposed surface.

Radiation effect; Microstructure; Polymers; LEFM

1. Introduction and background

Since their emergence in 1980s, polyureas have been gaining scientific and industrial attention leading to their implementation in many civilian and military applications, wherein impact mitigation is of a recent specific interest (Youssef and Gupta, 2012b; 2012a; Youssef, 2010). Generally, polyurea is a class of synthetic thermoset elastomer, formed by the poly-addition reaction of rapid crosslinking between an isocyanate and an oligomeric diamine. More specifically, viscoelastic polyurea is synthesized by mixing Versalink® P1000 with MDI Isocyanate in a ratio of 4:1, respectively, resulting in superior physical and mechanical properties including resistance to chemicals and moisture (Barsoum, 2015). For more than a decade now, this polyurea formulation has been highly investigated resulting in a culmination of the research efforts by Barsoum (2015), where he collated the major findings from many prominent mechanics groups around the United States. The superiority of the properties of this polyurea formulation is primarily attributed to the morphology, which corresponds to the microstructure comprising of interpenetrating hard and soft segments (Heyden et al., 2016). The hard domains provide the necessary reinforcement to the underlying microstructure and serve as physical crosslinks whereas the soft matrix provides the inherent flexibility in the polyurea structure (He et al., 2014). The morphology and the physical characteristics of polyurea are found to be affected by the segmental intermixing which is attributed to factors governing the polymerization reaction coupled with the stoichiometric ratio of the monomers as well as the chemical structure of the copolymer (He et al., 2014). In all, the broad range of mechanical response of polyurea is attributed to its complex microstructure.

Furthermore, the mechanical properties of polyurea are found to be strongly dependent on pressure and strain rate. Choi et al. (2012) found that under different quasi-static strain rates, the deformation beyond yield stress governed the orientation of the domains resulting in distortion of the hard segments with a subsequent reduction in phase segregation. Moreover, Yi et al. (2006) and Sarva et al. (2007) performed mechanical compression tests while Roland et al. (2007) performed tensile mechanical testing to elucidate the effect of strain rate. Regardless of the axiality of the applied stress, strong rate-dependent, nonlinear stress-strain behavior was observed. For both the tensile and compressive results, polyurea was found to transition from a rubbery state at low strain rates ($\sim 10^{-1}$ /s) to a glassy state at higher strain rates ($\sim 10^{3}$ /s). Guo et al. (2016) showed that the flow stress value of polyurea under compression is also dependent on the strain rate and temperature. They revealed that this interdependence of temperature and strain rate was less pronounced for materials under confined test conditions with the absence of yielding. In addition, Jiao et al. (2006) reported that polyurea was found to be insensitive to shearing rates ($\sim 10^{6}$ /s); however, it was highly dependent on the applied pressure, where an increase in pressure led to the increase in shearing resistance. Youssef and Gupta (2012) reported the spall strength of polyurea, under very high strain rate ($\sim 10^{7}$ /s) shock wave, to be 93.1 ± 5 MPa, indicating glassy behavior of polyurea at high strain rates.

Moreover, polyurea elastomeric coatings serve as an excellent adhesive that is impermeable to moisture, resilient to salinity, abrasions, variations in pH and ambient temperature (Kim et al., 2012). The intrinsic rate and pressure dependencies of polyurea have sparked active

* Corresponding author.
E-mail address: gyoussef@sdsu.edu (G. Youssef).

https://doi.org/10.1016/j.mechmat.2019.103244
Received 17 July 2019; Received in revised form 7 November 2019; Accepted 7 November 2019
Available online 08 November 2019
0167-6636/

research in the development of novel armor design due to the ability to tailor its underlying microstructure (Johnson, 1998). As a consequence of the applied pressure during a ballistic impact, the shearing resistance of polyurea was found to exceed that of a high strength steel thereby dissipating a significant amount of energy away from the impact along with the entrapment of destructive debris (Xue and Hutchinson, 2007; Bogoslovov et al., 2007). The superior ballistic impact mitigation of polyurea coatings is attributed to the second-order phase transition within the soft matrix (Bogoslovov et al., 2007; Grujicic et al., 2012), while the debilitation and dispersion of shock waves are associated with the hard segments (Grujicic et al., 2012; Grujicic and Pandurangan, 2012). Mohotti et al. (2013) further investigated that a polyurea coating on aluminum plates was found to significantly reduce the residual velocity of the projectile after impact. Grujicic et al. (2010), Gupta and Youssef (2014) also reported that the application of polyurea in athletic helmets was found to considerably reduce traumatic brain injuries at relatively high blast peak pressures. The eminence of polyurea in protective coating and impact mitigation application stipulates extended duration of exposure to ultraviolet radiation resulting in natural weathering.

As delineated above, polyurea has been thoroughly investigated over a decade for its versatility in various applications primarily in efficient armor design (Barsoum, 2015). Despite its superior mechanical properties and resistance to chemical attacks, the effect of extended ultraviolet (UV) radiation on polyurea has been scarcely investigated in recent years (Whitten and Youssef, 2016; Youssef et al., 2017; Youssef and Whitten, 2017). Whitten and Youssef (2016) recently reported that polyurea showed signs of discoloration and crack nucleation within 3 weeks of continuous exposure to UV radiation. Furthermore, the acoustic properties of UV-exposed polyurea were found to be affected by the extended exposure resulting in a drop of the shear wave attenuation at higher temperatures (Whitten and Youssef, 2016). Finally, the same group reported the effect of extended UV exposure on the dynamic and hyperelastic properties of polyurea (Youssef et al., 2017; Youssef and Whitten, 2017). Thus in the present work, the effect of extended UV radiation on the micromechanical properties of polyurea is evaluated and the results are explicated within a mechanics framework.

2. Experimental protocol

A multistep experimental protocol was designed with a focus on uncovering the overall effect of ultraviolet radiation on the microscale mechanical properties of the phase-segregated polyurea. The overall repeatability of the obtained results was ensured by taking measurements at three different locations of each sample.

2.1. Sample preparation

Polyurea sheets with a nominal thickness of 1 mm were prepared using a slab-molding technique by mixing a 4:1 wt ratio of diamine (© Bayville Chemical Versalink® P-1000 Oligomeric Diamine) and diisocyanate (© Bayville Chemical MDI Isonate™ 143 L), respectively. The mixture was then cured in a vacuum oven for 24 h at 80 °C (Whitten and Youssef, 2016). Subsequently, the polyurea sheet was removed from the mold and 30 circular discs of 25 mm in diameter were punched out and randomly sorted into nine sample sets. Eight of the sample sets were placed in the UV radiation exposure system while the remaining set was left unexposed and maintained as the control.

2.2. UV exposure setup

The UV exposure system (UVDOCTOR DDU2024) comprised of four equally-spaced bulbs with two different wavelengths of UV-A and UV-B radiation placed alternatively. The wavelength of the exposure system was between 290–480 nm with the peak wavelength of the bulbs being 360 nm and 420 nm for UV-B and UV-A, respectively. The exposure system was enclosed with mirror-finished stainless steel panels to reflect the UV radiation uniformly onto the samples. The samples were elevated from the bottom surface to further ensure homogenous exposure by placing them on a UV transparent acrylic. The first sample set was removed after 1.5 weeks of exposure, while the remaining sets were removed after 3, 4.5, 6, 7.5, 9, 12 and 15 weeks, consecutively. The energy radiated by the system was measured to be 5.1 J/cm^2 per hour of UV-A and 8.5 J/cm^2 per hour of UV-B using a UV radiometer (Power Puck-II) (Whitten and Youssef, 2016).

2.3. Surface roughness characterization

Surface roughness characterization of the UV-exposed polyurea samples were performed using an Atomic Force Microscope (TT2 - AFM Workshop) operating in the tapping mode under ambient conditions. Silicon probes (Appnano – ACLA, k = 22 N/m R_o = 160 kHz) having a reflective aluminum coating with a tip radius of 15 nm, as reported by the manufacturer, were used. Scans were obtained at moderate tapping forces with the free air amplitude and set point being 1.5 V and 0.9 V, respectively. The set point to free air amplitude ratio (R_{sp} ratio) was maintained at 0.6–0.7 to prevent excess probe wear and to avoid measurement artifacts that may result in errors in the obtained data, which were observed at a lower R_{sp} ratio. Samples with an area of 50 × 50 μm^2 were randomly selected and scanned at a spatial resolution of ~49 nm/line to capture the surface roughness at the highest resolution. The scans obtained were corrected for tilt by first-order plane leveling using Scanning Probe Microscopy (SPM) analysis software (Gwyddion), thereafter the root mean square (RMS) of the sample surface roughness was calculated and reported.

2.4. Crack measurements

The crack opening (referring to the distance separating the crack surfaces at the surface of the sample) measurements were performed using high aspect ratio tips (Bruker TESP – HAR, k = 72 N/m, R_o = 320 kHz) with non-reflective coating and a reported tip radius of 10 nm. The free air amplitude and the set point were adjusted to 1.5 V to 0.75 V, respectively. An R_{sp} ratio of 0.5 – 0.6 was maintained to effectively engage the tip with the surface and to prevent tip lift-off while scanning around the crack edge. Following surface reconnaissance to locate the largest cracks, three areas of each sample were selected using an optical microscope. An AFM scan of 40 × 40 μm^2 was obtained around each crack area, with the exception of the 15-week samples, which were scanned at 50 × 50 μm^2 to accommodate the significant increase in the crack opening. The crack opening was quantified by measuring the distance between the crack edges using SPM software (Gwyddion). The vertical sensitivity of the equipment limited the capability of the AFM to quantify the large crack length since our AFM has a total vertical displacement of 17 μm, which translates to 8.5 μm of out-of-plane travel above and below the static equilibrium position of the cantilever; a physical limitation overcome by SEM as discussed next. A total of nine scans were obtained per exposure duration at different crack sites, which were located sufficiently apart from one another for statistical significance.

On the other hand, changes in crack length (referring to the extension of the crack into the sample perpendicular to the surface) were measured using SEM (FEI Quanta 450) by obtaining transverse sections of the samples. The transverse sections of the polyurea discs were sliced at room temperature using a fresh, sharp blade, thus, avoiding the use of excessive mechanical force as seen in using a microtome or cutting a brittle solid at cryogenic temperatures. This procedure prevented the formation of any new cracks that were not induced by the extended ultraviolet radiation. The sections were then mounted in an acrylic solution (cured at room temperature) to maintain perpendicularity during scanning. At least ten different crack length measurements were

obtained for each sample set. The crack growth was quantified by modeling the cracks as Mode I cracks in semi-infinite continuum using Linear Elastic Fracture Mechanics (LEFM) due to tensile stress acting along the plane of the sample resulting from the surface shrinkage strain based on the extended UV exposure.

2.6. Microscale force – distance measurements

Local modulus measurements were obtained using the atomic force microscope fitted with high sensitivity (Bruker RTESP – 300, k = 200 N/m, R_o = 550 kHz) silicon probes with a reflective aluminum coating in contact mode. The probes have a reported tip radius of 8 nm by the manufacturer, which was independently verified using scanning electron microscopy of the tip. The spring constant of the cantilever was obtained using the Sader method (Sader et al., 1999) and was found to be 98 N/m. The average deflection sensitivity of the cantilever was found to be 280 nm/V by using a silicon wafer for calibration. A total of 16 force-displacement plots were collected in a selected area of 10 × 10 μm^2 with minimal surface defects and impurities to prevent discrepancy in the obtained data. A maximum force of 4 μN was maintained by adjusting the retract voltage of the photodetector. The travel of the probe was defined with a step size of 1.6 nm throughout the measurement process. Three random locations were selected for each sample set, thus a total of 48 plots were obtained per exposure duration. Fig. 1a shows a representation of the extend/retract curve highlighting the major characteristics of an AFM force-distance curve. Additionally, Fig. 1b includes a realistic exemplary data from characterizing the force-distance of a 15-weeks sample, which clearly demonstrates the interaction between the tip and surface of the sample beyond the roughness.

The local modulus of the samples was calculated by fitting the retract force-displacement curve onto the Derjaguin, Muller, Toporov (DMT) model. The DMT model was selected since it takes into account the adhesive forces between the tip and the sample, which makes it suitable for analyzing contact of soft materials such as polymers. The DMT model is valid for stiff contact of the tip with a flat substrate in ambient conditions; such an assumption is congruent with the experimental conditions used herein. It is worth noting that other fitting models were initially considered but the DMT model was found to perform reasonably given the focus of the research herein (Maugis, 1992; Johnson, 1998). Nonetheless, future research can focus on parametrically delineating any possible discrepancy between all available models. The reduced modulus (E_r) defined by the DMT fit is given by

$$F - F_{adh} = \frac{4R}{3E_r}\sqrt{Ra^3} \tag{1}$$

where, a is the contact radius, R is the tip curvature radius, F is the cantilever force, and F_{adh} is the adhesion force. Therefore, the elastic modulus of the degraded surface layer is then given by

$$\frac{1}{E_r} = \frac{(1-\nu_s^2)}{E_s} + \frac{(1-\nu_c^2)}{E_c} \tag{2}$$

where, E_s, ν_s and E_c, ν_c are the elastic modulus and Poisson's ratio of the sample (taken to be 0.5 during the data reduction process) and the cantilever, respectively. Since the tip is much stiffer than the sample, the second term on the right-hand side of Eq. (2) can be neglected. This assumption was validated by calculating the local elastic modulus with and without the second term in Eq. (2), the difference between the results was found to be negligible.

In addition to using the retract curve to calculate the local elastic modulus, the contact stiffness represented by the slope of the force-distance retract line was used to forecast the changes in polyurea due to extended UV exposure. A comparative stress measure, ς, was calculated by dividing the square of the contact stiffness by the applied load.

3. Results and discussion

3.1. Surface roughness

The evolution of the surface morphology and topography of polyurea as a function of extended UV radiation are shown first qualitatively in Fig. 2, where the overall surface degradation is evident from the AFM micrographs. After the initial 1.5 weeks of continuous exposure, incipient nanoscale cracks and micro-voids manifest on the surface, however, the grainy undersurface structure present on the surface micrograph of the unexposed sample is still clearly recognizable. Thereafter, the crack density continues to increase until it almost covers the entire surface, which is observed by studying micrographs of 3, 4.5, 6 weeks of UV exposure. In other words, the 2–4 μm micro-cracks visible after 1.5 weeks progressively lead into sample-wide crazing after three weeks. At 7.5 weeks of UV exposure, chalking of the sample can be observed along with broadening of the initial cracks and nucleation of side micro-cracks as well as an increase in surface irregularities until 15 weeks of exposure.

The UV-induced crazing is reported to be primarily a surface phenomenon of local stress relief since surface traction cooperatively induced by embrittlement of the surface initiating shrinkage strain. The limitation of crazing to the surface was previously reported (Youssef and Whitten, 2017) and is confirmed by dark-field optical microscopy analysis of the sample cross-section. Notably, crazing

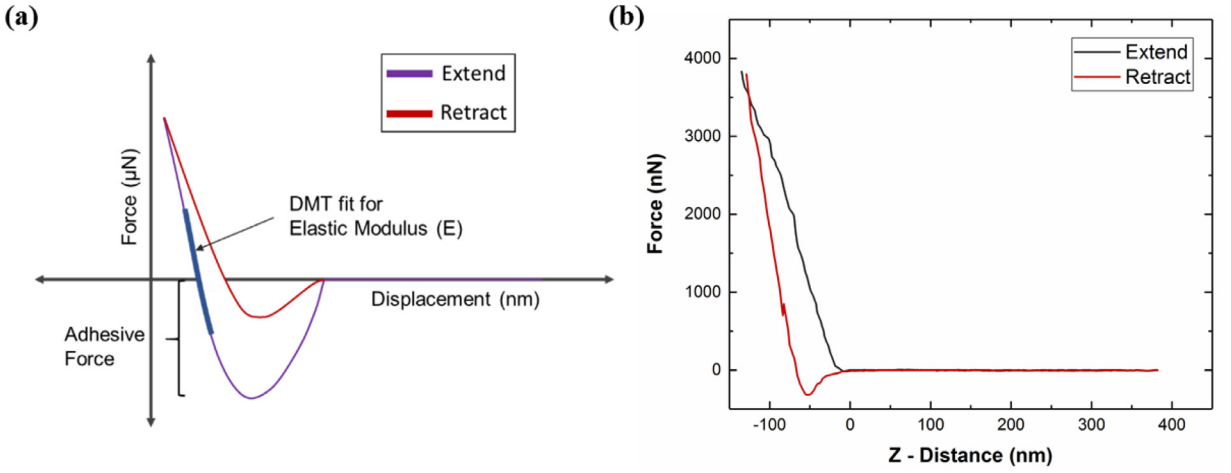

Fig. 1. (a) Graphical representation of Force-Distance curve with DMT fit and (b) a realistic example of collected data from testing 15-weeks sample.

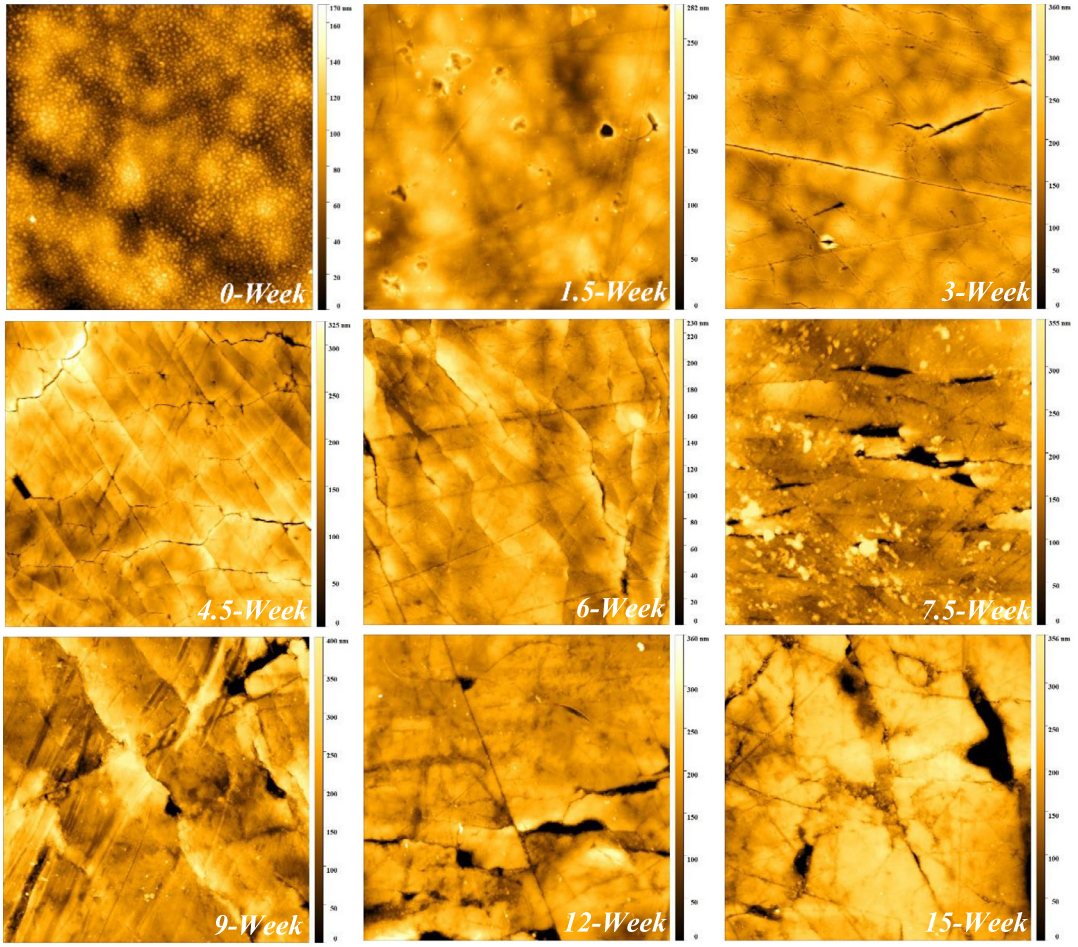

Fig. 2. AFM micrographs of 50 × 50 μm^2 (i.e., a square area with side dimension of 50 μm) showing the surface morphology and topography (scale shown on the right of each scan) of the UV irradiated polyurea.

necessitates a stress field at levels of the tensile strength (corresponding to high strain testing, i.e., brittle behavior) to form and grow (Argon, 2013). That is, as Argon discussed, the initiation and growth (thickening and propagation) of crazes are an interplay between the stress-tensor invariants, namely deviatoric and mean normal stress components (Argon, 2013). The incipient nano- and macro-scale cracks and voids are first produced by the compliant nature of the polyurea through the deviatoric shear component, which is consecutively expanded by the normal mean stress component. Once the initial cracks are created, when the stress field is in excess of the tensile strength, these new cracks act as stress-concentrators leading to the increase in crack density and distribution as discussed before and shown in Fig. 2. Here, the stress field that instigates the crazing process is a byproduct of the shrinkage strain prompted by the byproducts of photo-oxidation reaction resulting in increased oxygen diffusion during the UV exposure process (Argon, 2013).

Fig. 3 quantitatively summarizes the progressive step-wise increase in the surface roughness of UV-radiated polyurea samples with respect to the exposure duration. Also reported, the RMS of the surface roughness calculated based on measuring 50 × 50 μm^2 scans of three locations on each sample. RMS roughness was found to follow the same step-wise increments as the average surface roughness. However, the magnitude is higher than the arithmetic mean surface roughness since RMS is more sensitive to surface variation. The RMS surface roughness of the virgin sample was found to be below 50 nm, with a slight increase after 1.5 weeks of exposure. This signified a total increase of 220% after 15 weeks of exposure at an extrapolated approximate rate of 6.9 nm per each week of exposure. The abrupt increase in surface roughness after 3

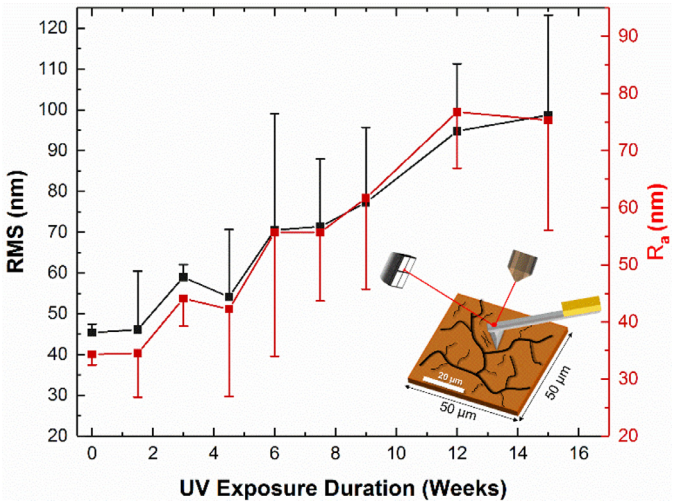

Fig. 3. Progressive increase in the surface roughness of polyurea as a function of exposure duration.

weeks corresponds to the onset of increase in the local modulus (discussed later), thereafter freshly exposed polyurea (within the crack surface) soften the overall behavior by relieving the normal stress buildup on the surface due to the underlying photo-oxidation process stemming from the interaction between degrading ultraviolet radiation and exposed surface of polyurea. In general, photo-oxidation is a

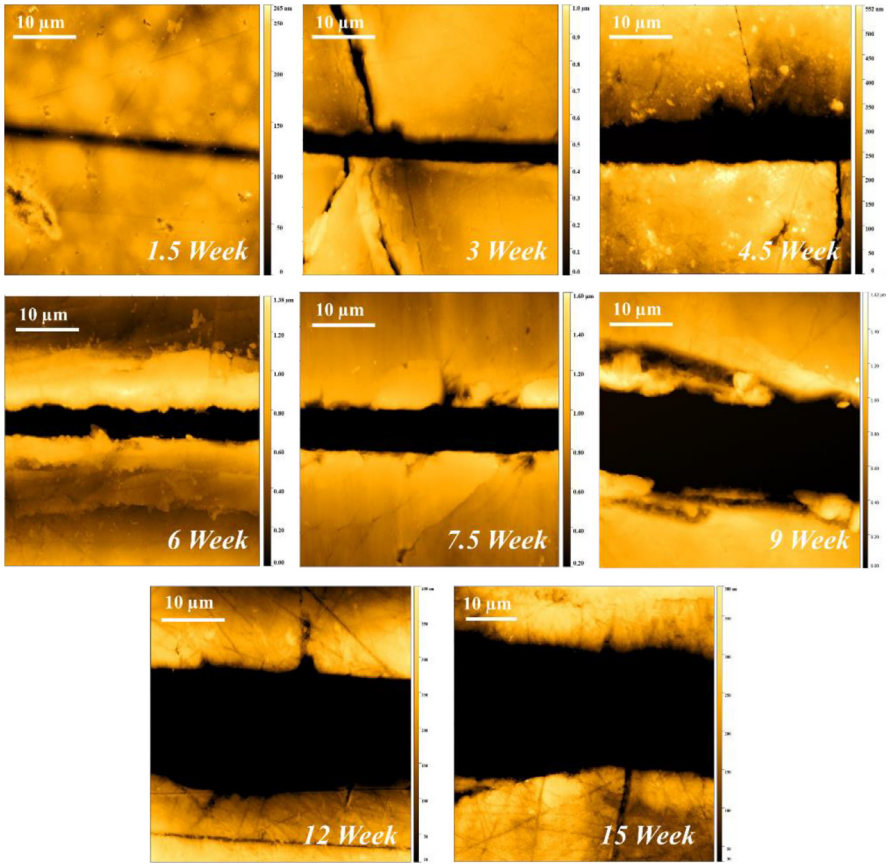

Fig. 4. AFM micrographs of 50 × 50 μm^2 of 15 Week and 40 × 40 μm^2 from 1.5 Week −12 Week showing the crack profiles of the UV irradiated polyurea.

surface aging process, where the ductile core of the sample is masked by a surface degraded embrittled layer.

3.2. Crack characteristics

To observe the effects of UV radiation on the crack growth, AFM scans of the crack opening were obtained using the protocol delineated in Section 2.4. The micrographs in Fig. 4 reveal progressive crack widening throughout the course of exposure, which is prompted by the cumulative internal strain buildup. Each of the subgraphs in Fig. 4 was collected from a different sample that was extracted from the specimen set corresponding to different exposure duration. The onset of crazing within 3 weeks of exposure instigated by the combined effect of plastic relaxation and increased surface traction force, which progressively resulted in longitudinal cracks formation. Mud cracking was observed as early as after 4.5 weeks of exposure accompanied by the skin shrinkage of the island region between the cracks subsequently yielding wider cracks throughout the exposure. The AFM scans also revealed the initial smooth edges of the cracks suggesting brittle failure. This could be caused by the segregation of the hard and soft phases in polyurea, where the soft amorphous matrix has lower bond energy crystallized due to the extended UV exposure and generates smoother crack edges. These measurements have been further quantified in Fig. 5, which presents the average crack opening of a total of nine AFM scans per each exposure week. As observed in Fig. 5, the average crack opening of the UV-exposed polyurea samples over the entire duration of exposure shows an extrapolated average crack growth rate of 1.8 μm/week. This continual widening of the cracks, as explained earlier, arises from the increased shrinkage resulting in higher oxygen uptake sustaining photo-oxidation reaction.

The crack length measurements are quantitatively summarized in Fig. 6, which shows three different growth rates as a function of the

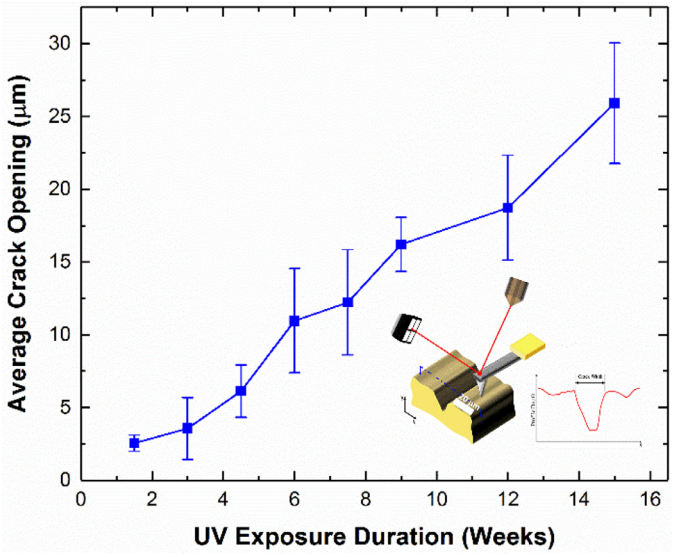

Fig. 5. Effect of extended UV radiation on the crack opening of the surface of polyurea.

exposure duration. First, a linear increase in the crack length is observed to be a rate of 6.8 μm/week from the third week until the sixth week of exposure. After that, the cracks appear to be arrested at the core of the sample and remained mostly unchanged until the twelfth week with a mere growth of 1.2 μm/week. This drop is likely caused by the oxygen gradient limited to the bottom of the crack, thereby subsequently slowing the reaction. Finally, once the newly formed crack surfaces are exposed to extended UV radiation, the arrested cracks start

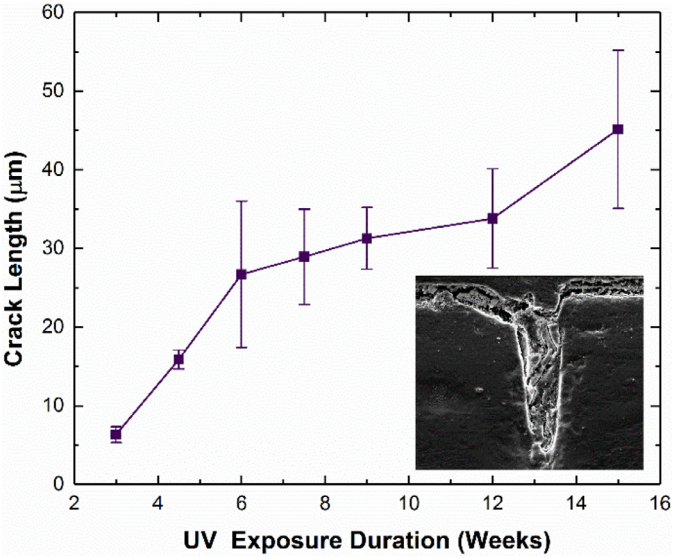

Fig. 6. SEM crack length measurements (inset shows a micrograph of crack captured from 15-week samples).

to propagate again at a rate of 5.8 μm/week as shown after 12 weeks until the end of the exposure duration.

To gain insights into the aforementioned fracture process, LEFM framework was leveraged for the subsequent analysis, which was justified since crack initiation and propagation occurred in the embrittled layer of polyurea and became arrested in the bulk viscoelastic core preventing further propagation until oxygen diffused into the depth. In other words, once the degradation occurs, the media surrounding the crack tip is unable to resist the stress buildup around the tip and further crack propagation continues only to be arrested again within a fresh viscoelastic core that was not exposed to UV radiation as it was masked by the UV-degraded surface layer. That is, the nature of brittle failure making it a Mode I cracking and the assumptions of LEFM of the top highly-degraded surface layer being linear, elastic, and isotropic material are within the investigated framework.

Current cracking of the sample is considered as parallel edge cracking in a half-plane subjected to in plane stress with a semi-infinite row of normal edge cracks loaded in tension, see inset of Fig. 7 for a schematic representation of the considered problem. The stress intensity factor, K_I, characterizes the magnitude of the applied stress near the crack tip and is defined as

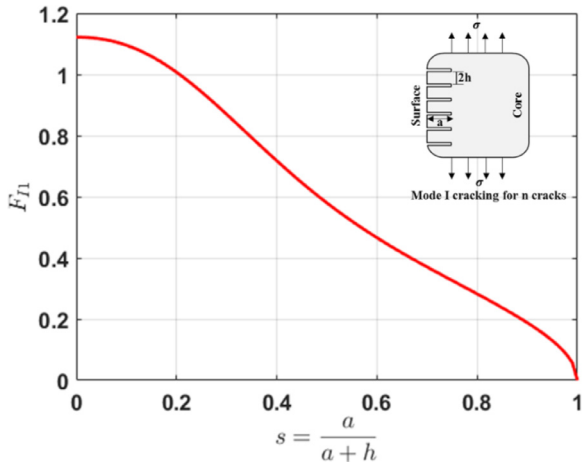

Fig. 7. Geometrical factors for parallel edge cracks reproduced after (Sih, 1973).

$$K_I = \sigma\sqrt{\pi a}\,F_{11}(a, n) \tag{3}$$

where, $\boldsymbol{\sigma}$ is the applied stress in MPa and **a** is the crack length in mm, which was measured using SEM. F_{11}(a,n) is a geometrical correction function for the crack geometry, which is dependent on the ratio of crack length to specimen width and $n = \frac{L}{2h}$ is the total number of transverse cracks (h is the half distance between two adjacent cracks). The geometrical correction factor (F_{11}) is obtained by implementing numerical interpolation between asymptotic expansions given by s which is the ratio of crack length to crack length plus the half distance between two adjacent cracks. To minimize the error, the geometric correction factor F_{11} is approximated by a 10th order polynomial with an error of 1–2% which is given by Eq. (4) and shown graphically in Fig. 7 (Sih, 1973).

$$F_{11} = \frac{1}{\pi^{\frac{1}{2}}}\left[1 + \frac{1}{2}\frac{h}{s} + \frac{3}{8}\frac{h^2}{s^2} + \frac{5}{16}\frac{h^3}{s^3} + \frac{35}{128}\frac{h^4}{s^4} + \frac{63}{256}\frac{h^5}{s^5} + \frac{231}{1024}\frac{h^6}{s^6}\right] + 22.501\frac{h^7}{s^7} - 63.502\frac{h^8}{s^8} + 58.045\frac{h^9}{s^9} - 17.577\frac{h^{10}}{s^{10}} \tag{4}$$

Thus, the estimation of the critical stress intensity factor can be done by using the tensile strength of polyurea as well as the periodicity of the crack measured from the SEM micrographs of the cross-sections. The periodicity is reported based on measuring the crack spacing along the entire cross section of one sample from each set of exposure duration. Due to the shallowness of the cracks within the first three weeks of exposure, the periodicity was not easily resolved using the SEM. Youssef et al. previously reported the former as the dynamic tensile strength (93.1 MPa) when polyurea was tested at a strain rate of $10^7\ s^{-1}$, which is taken to be the strength of the brittle (glassy) material (Youssef and Gupta, 2012). The adoption of the dynamic strength, which was measured of unexposed sample at ultrahigh strain loading conditions, for the current analysis framework is reasonable based on twofold justification. First, testing under ultrahigh strain rate suppresses all inelastic deformation mechanisms (e.g., creep and yielding), hence the material does not have time to undergo plastic deformation and fails in a brittle fashion. Second, the crack tip at the onset of propagation is most likely situated within the brittle surface layer. The crack periodicity was found to be 79.2, 55.3, 49.5, 50.6, 47.9 and 27.5 μm for exposure durations of 4.5, 6, 7.5, 9, 12 and 15 weeks, respectively. The periodicity for 1.5 and 3 weeks were proven difficult to acquire using the SEM due to the shallowness of the cracks and lack of crack directionality early in the exposure process. Hence, by making no assumptions about the crack length (i.e., a variable that was numerically varied), the stress intensity factor was calculated using Eq. (3) (by plugging in the assumed crack length and the strength values discussed above) and Eq. (4) (by calculating the new geometrical factor based on the assumed crack length) by incrementally increasing assumed values of the crack length. It was found that K_I starts to increase as the assumed value of the crack length ascended, until K_I reached a maximum (see Fig. 8a for an illustration of this explanation; the example shown is for 15 weeks but other exposure duration exhibited identical response but different values of crack length and K_I). The maximum value of K_I was taken to be the plane-stress critical stress intensity factor (K_C) and the corresponding crack length was considered to be the critical crack size prompting further propagation. The estimated critical stress intensity factor and the corresponding crack length are shown in Fig. 8b. The results show that the critical crack length deduced from the K_C calculation was found to match closely with those reported experimentally using the SEM (see Fig. 6). In all, the critical stress intensity factor for embrittled polyurea layer was found to be 0.49 ± 0.08(SD) $MPa.m^{0.5}$.

3.3. Force-distance measurements

The microscale (local) elastic moduli obtained from the curve fitting of the force-displacement curves of the exposed samples are

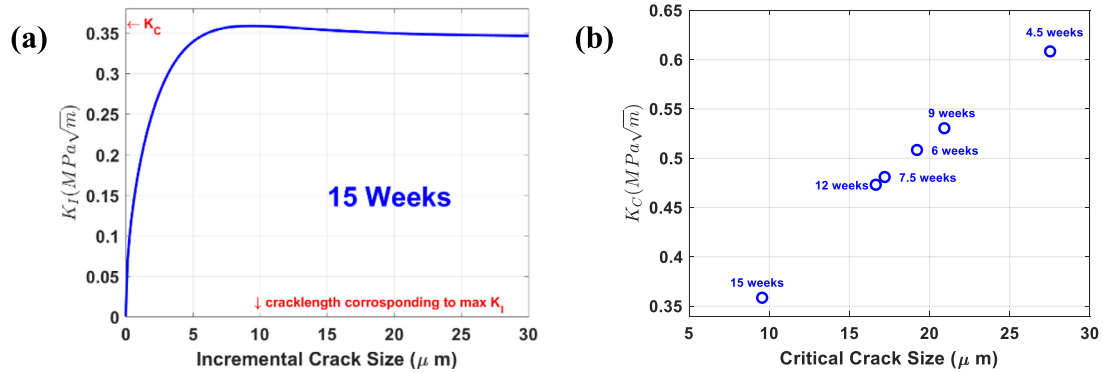

Fig. 8. (a) An example (for 15 weeks) of the output of the algorithm used to obtain the critical stress intensity factor and (b) plane stress critical stress intensity factor for Mode I parallel edge crack reported as function of critical crack size.

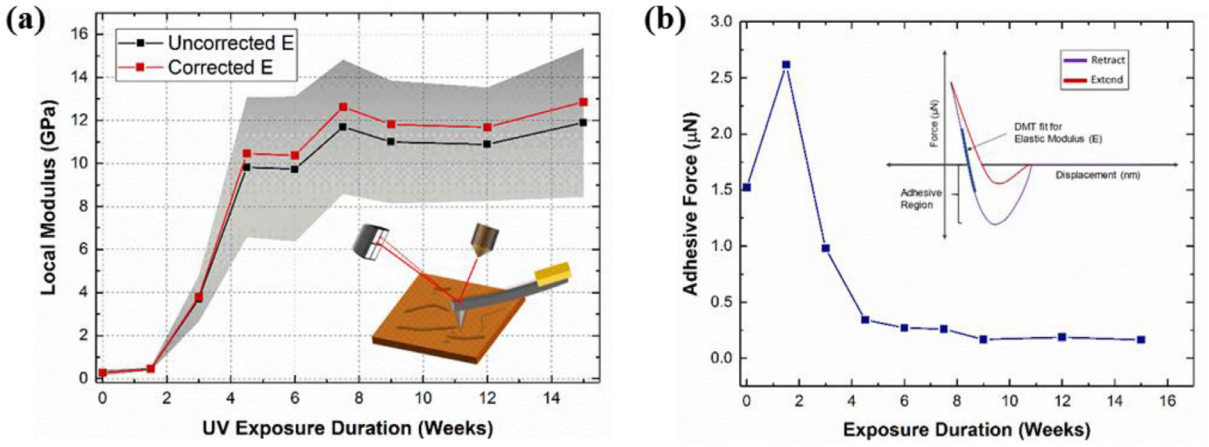

Fig. 9. The evolution of (a) local modulus and (b) adhesion force of UV-exposed polyurea.

summarized in Fig. 9a and the corresponding adhesion forces calculated during the retract phase are reported in Fig. 9b. The results indicate a similar observation to those noted previously, where a nearly eightfold increase in material stiffness was reported after 3 weeks in comparison to 1.5 weeks of continuous exposure. Further exposure resulted in a corresponding increase in the modulus until 7.5 weeks; thereafter, it remained mostly unchanged until the end of the exposure duration. Fig. 9a shows two renditions of the local elastic modulus by considering (corrected) and neglecting (uncorrected) cantilever stiffness, i.e., the second term on the right-hand side of Eq. (2). The uncorrected local modulus of the virgin sample was 0.27 ± 0.12 GPa with an incremental uptick to 3.71 ± 1.07 GPa and 9.832 ± 3.25 GPa after 3 and 4.5 weeks, respectively. The local surface modulus reached a maximum of 11.9 ± 3.46 GPa after 15 weeks of continuous UV exposure. The corrected microscale modulus was found to be in close agreement, further verifying the validity of neglecting the effect of the mechanical properties of the cantilever beam on the reported measurements.

The increase in the stiffness of the exposed samples is attributed to the decrease in the viscous dampening (shown in Fig. 9a) of their viscoelastic response. The tip-sample adhesion forces of the exposed samples (Fig. 9b) were found to increase until 1.5 weeks, thereafter dropping drastically after 3 weeks of exposure. While fresh, unexposed polyurea surface had an adhesion force of 1.5 μN which significantly dropped to 0.17 μN after 9 weeks of exposure and attenuated thereafter. The initial increase in tip-sample adhesive forces is thought to be attributed to the initial effect of ultraviolet radiation on the surface of polyurea through chain scission hence creating free radicals that attracts the tip towards the sample. As the exposure duration increases, the photo-oxidation continues (since the exposure apparatus was not sealed) resulting in an increased surface embrittlement and the sudden drop in the adhesive force. A similar study on thermal degradation of EPDM (terpolymer ethylene-propylene-diene monomer) has also shown changes in mechanical properties with the increase in exposure duration (Kumar et al., 2004).

The experimental results of the crack opening can be further elucidated using the framework of LEFM since the local elastic modulus and the estimated critical stress intensity factor as function of weeks of exposure are now reported. As discussed above, the crack opening seems to exhibit two large changes corresponding to weeks 4.5 and 12 followed by a slow (stable) progression, which can be better explicated from Fig. 5. It is to say, once the energy at the crack tip reaches a critical value, also refer to as the energy release rate, the arrested crack has enough energy to overcome the cohesion strength of the material and propagates, thus resulting not only in an increase in the crack length (as shown in Fig. 6) but also an increase in the crack opening (Fig. 5). Under the current loading scenario, i.e. stresses developed due to weathering causing crazing, as seen in Fig. 5, the crack before 6 weeks of exposure appears to propagate rapidly then gets arrested again between 6 and 12 weeks, as previously discussed. Thereafter, the crack tip accumulate enough energy to repeat the same process at 12 weeks.

Before furthering the discussion about the crack opening, it is fitting to validate the previously reported critical stress intensity factor and we do so by recalling the relationship between the K_C and crack opening (δ) from LEFM such that

$$K_C = \sqrt{\delta \lambda E \sigma_y} \tag{5}$$

Here, the elastic modulus (E) is given in Fig. 8. The yield strength (σ_y) was reported by Brinson for the same polyurea composition as a function of ultraviolet radiation, which was found to be between 2.35 and

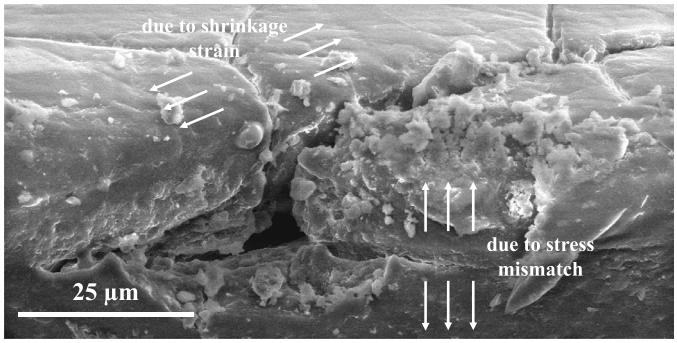

Fig. 10. SEM micrograph of the interfacial crack of a 15-week sample (modified after (Youssef and Whitten, 2017)).

2.25 MPa for 4.5 weeks and 2.08 MPa 12 weeks (Brinson, 2013). Furthermore, the inset of Fig. 6 shows an SEM micrograph of a crack without any evidence of fibrils bridging between the crack surfaces therefore indicating brittle fracturing in the material. Thus, the value of λ in Eq. (5) is taken to be 1 (Meyers and Chawla, 2009). Plugging the values of the corresponding elastic modulus and yield strength into Eq. (5) at 4.5 and 12 weeks result in a stress intensity factor of 0.43 MPa $m^{0.5}$ and 0.42 MPa $m^{0.5}$, respectively. These calculated values for K_C (based on Eq. (5)) were found to be in a reasonable agreement with the average value of K_C (based on Eq. (3)) within a 12% difference. Despite the reasonable agreement in the results of K_C using Eq. (3) and Eq. (5), it is important to note that the fracture behavior of the bilayer UV-exposed/virgin core polyurea sample is interdependent on the evolution of crack geometry, yield strength, tensile strength, and the microstructure, to name a few, as function of ultraviolet exposure duration.

Additionally, the realm of LEFM offers another insight into the above reported data pertaining to the crack opening (δ_c) since it is related to the elastic modulus and the critical stress intensity factor (in-plane stress conditions) such that

$$\delta_c = \frac{K_C{}^2}{\lambda E \sigma_y} \tag{6}$$

Taking the values discussed above for the variables in Eq. (6), the calculated critical crack opening corresponding to weeks 4.5 and 12 (i.e., unstable crack propagation) were found to be 8.3 μm and 10.9 μm, which is in good agreement with the experimental results reported in Fig. 5.

Finally, the evolution of interfacial cracks, i.e. a measured increase of 5 μm and 50 μm in crack length and crack width, respectively, between the 12-week and 15-week samples, was previously reported by Youssef and Whitten (2017), can now be explicated using LEFM with the help of the first Dundurs' parameter (α) (Yakimets et al., 2004). Fig. 10 shows a micrograph of a 15-week sample with a crack length and width of approximately 25 μm and 66 μm, respectively (Youssef and Whitten, 2017).

It is worth noting that such predictions were not previously possible due to the lack of measurements of local material stiffness corresponding to the duration of UV exposure. The elastic mismatch based on the difference in the moduli between the degraded (E_D) and virgin (E_C) polyurea as it compares to the total stiffness of these layers is defined as the Dundurs' parameter given by Eq. (7).

$$\alpha = \frac{(E_D - E_C)}{(E_D + E_C)} \tag{7}$$

In other words, the disparity between the exposed and unexposed moduli gives rise to an elastic mismatch resulting in nucleation of cracks at the interface between ultraviolet-degraded layer and the unexposed core. This phenomenon can be clearly elucidated by considering the Dundurs' parameter of 0.87, which was calculated based on the moduli ratio of 0.073 between the virgin polyurea and samples after 3 weeks of exposure. In contrast, the Dundurs' parameter for moduli ratio of 0.62 corresponding to 1.5 weeks of exposure is only 0.24, indicating the unlikelihood of interfacial crack to form and propagate at such low level of exposure. Finally, the Dundurs' parameter remained relatively constant at 0.94 after 4.5 weeks of exposure at a moduli ratio of 0.028 and continued at nearly the same value until the overall duration of exposure, indicating high probability of interfacial crack formation.

4. Conclusion

In the present work, the effect of UV radiation upon the microstructure of polyurea is reported. The changes in surface morphology arising from the extended UV exposure in ambient conditions were evident throughout the overall duration of exposure. Crazing within the third week of exposure resulting from the byproducts of the photo-oxidation reaction progressively increased the surface roughness of the polyurea samples. The average crack opening increased linearly until the fifteenth week of exposure as a result of the increased surface traction force arising from the increasing shrinkage strain due to surface embrittlement. Formation of mud cracking was evident after 4.5 weeks, thus exposing more compliant polyurea causing subsequent crack growth. Crack morphology observed from the AFM micrographs revealed sharp edges indicating brittle failure, which was further evaluated from the AFM force-distance plots. The local elastic modulus increased considerably after the third week and peaked after 7.5 weeks of exposure while remaining largely unaffected for the rest of the duration. Similar results were obtained from the tip-sample adhesive forces, where a significant drop was observed after an exposure duration of four and a half weeks with a very small drop thereafter indicating significant loss in viscous damping. A LEFM framework was employed to explicate the fracture behavior of the surface crack due to extended UV exposure. Finally, the Dundurs' parameter obtained by reducing the local moduli suggested a high probability of formation of interfacial cracks arising from the stress mismatch between the degraded brittle surface and soft sample core. These results signify the drastic impact of extended UV radiation on the microstructure of virgin polyurea, which under high impact stresses could compromise its structural integrity due to the propagation of UV induced cracks into the core resulting in premature failure. This study thereby incites interest in understanding the synergistic impact of temperature, humidity and extended UV radiation on the microstructural and viscoelastic properties and their effect on the impact mitigation property of polyurea.

Declaration of Competing Interest

We wish to declare that there are no known conflict of interest associated with this publication.

Acknowledgment

The research leading to these results was supported in part by the United States Department of Defense under Grant Agreement No. W911NF1410039 and W911NF1810477. The research was also supported by internal funds from San Diego State University. The authors also acknowledge the use of equipment at the San Diego State University Electron Microscopy Facility acquired by NSF instrumentation grant DBI-0959908.

References

Argon, A.S., 2013. The physics of deformation and fracture of polymers. Cambridge University Press, New York. https://doi.org/10.1017/CBO9781139033046.
Barsoum, R.G., 2015. Elastomeric Polymers with High Rate Sensitivity. Applications in

Blast, Shockwave, and Penetration Mechanics, Elsevier Inc, Waltham, MA. https://doi.org/10.1016/B978-0-323-35400-4/00011-8.
Bogoslovov, R.B., Roland, C.M., Gamache, R.M., 2007. Impact-induced glass transition in elastomeric coatings. Appl. Phys. Lett. 90. https://doi.org/10.1063/1.2745212.
Brinson, J., 2013. Ultra-violet radiation effect on the mechanical properties of polyurea. California State University, Northridge.
Choi, T., Fragiadakis, D., Roland, C.M., Runt, J., 2012. Microstructure and segmental dynamics of polyurea under uniaxial deformation. Macromolecules 45, 3581–3589. https://doi.org/10.1021/ma300128d.
Grujicic, M., Bell, W.C., Pandurangan, B., He, T., 2010. Blast-wave impact-mitigation capability of polyurea when used as helmet suspension-pad material. Mater. Des. 31, 4050–4065. https://doi.org/10.1016/j.matdes.2010.05.002.
Grujicic, M., D'Entremont, B.P., Pandurangan, B., Runt, J., Tarter, J., Dillon, G., 2012. Concept-level analysis and design of polyurea for enhanced blast-mitigation performance. J. Mater. Eng. Perform. 21, 2024–2037. https://doi.org/10.1007/s11665-011-0117-8.
Grujicic, M., Pandurangan, B., 2012. Mesoscale analysis of segmental dynamics in microphase-segregated polyurea. J. Mater. Sci. 47, 3876–3889. https://doi.org/10.1007/s10853-011-6243-8.
Guo, H., Guo, W., Amirkhizi, A.V., Zou, R., Yuan, K., 2016. Experimental investigation and modeling of mechanical behaviors of polyurea over wide ranges of strain rates and temperatures. Polym. Test 53, 234–244. https://doi.org/10.1016/j.polymertesting.2016.06.004.
Gupta, V., Youssef, G., 2014. Orientation-Dependent impact behavior of polymer/eva bilayer specimens at long wavelengths. Exp. Mech. 54, 1133–1137. https://doi.org/10.1007/s11340-014-9854-6.
He, Y., Xie, D., Zhang, X., 2014. The structure, microphase-separated morphology, and property of polyurethanes and polyureas. J. Mater. Sci. 49, 7339–7352. https://doi.org/10.1007/s10853-014-8458-y.
Heyden, S., Ortiz, M., Fortunelli, A., 2016. All-atom molecular dynamics simulations of multiphase segregated polyurea under quasistatic, adiabatic, uniaxial compression. Polymer 106, 100–108. https://doi.org/10.1016/j.polymer.2016.10.053.
Jiao, T., Clifton, R.J., Grunschel, S.E., 2006. High strain rate response of an elastomer. AIP Conf. Proc. 845 II, 809–812. https://doi.org/10.1063/1.2263445.
Johnson, K.L., 1998. Mechanics of adhesion. Tribol. Int. 31, 413–418. https://doi.org/10.1016/S0301-679X(98)00060-7.
Kim, H., Citron, J., Youssef, G., Navarro, A., Gupta, V., 2012. Dynamic fracture energy of polyurea-bonded steel/E-glass composite joints. Mech. Mater. 45, 10–19. https://doi.org/10.1016/j.mechmat.2011.08.017.
Kumar, A., Commereuc, S., Verney, V., 2004. Ageing of elastomers: a molecular approach based on rheological characterization. Polym. Degrad. Stab. 85, 751–757. https://doi.org/10.1016/j.polymdegradstab.2003.11.014.
Maugis, D., 1992. Adhesion of spheres: the JKR-DMT transition using a Dugdale model. J. Colloid Interface Sci. 150, 243–269. https://doi.org/10.1016/0021-9797(92)90285-T.
Meyers, M.A., Chawla, K.K., 2009. Mechanical Behavior of Materials, 2nd ed. Cambridge.
Mohotti, D., Ngo, T., Mendis, P., Raman, S.N, 2013. Polyurea coated composite aluminium plates subjected to high velocity projectile impact. Mater. Des. 52, 1–16. https://doi.org/10.1016/j.matdes.2013.05.060.
Roland, C.M., Twigg, J.N., Vu, Y., Mott, P.H., 2007. High strain rate mechanical behavior of polyurea. Polymer 48, 574–578. https://doi.org/10.1016/j.polymer.2006.11.051.
Sader, J.E., Chon, J.W.M., Mulvaney, P., 1999. Calibration of atomic force microscope cantilevers. Rev. Sci. Instrum. 70, 3967–3969.
Sarva, S.S., Deschanel, S., Boyce, M.C., Chen, W., 2007. Stress-strain behavior of a polyurea and a polyurethane from low to high strain rates. Polymer 48, 2208–2213. https://doi.org/10.1016/j.polymer.2007.02.058.
Sih, G.C., 1973. Methods of Analysis and Solutions of Crack Problems: Recent Developments in Fracture Mechanics. Noordhoff International Pub, Leyden.
Whitten, I., Youssef, G., 2016. The effect of ultraviolet radiation on ultrasonic properties of polyurea. Polym. Degrad. Stab. 123, 88–93. https://doi.org/10.1016/j.polymdegradstab.2015.11.009.
Xue, Z., Hutchinson, J.W., 2007. Neck retardation and enhanced energy absorption in metal-elastomer bilayers. Mech. Mater. 39, 473–487. https://doi.org/10.1016/j.mechmat.2006.08.002.
Yakimets, I., Lai, D., Guigon, M., 2004. Effect of photo-oxidation cracks on behaviour of thick polypropylene samples. Polym. Degrad. Stab. 86, 59–67. https://doi.org/10.1016/j.polymdegradstab.2004.01.013.
Yi, J., Boyce, M.C., Lee, G.F., Balizer, E., 2006. Large deformation rate-dependent stress-strain behavior of polyurea and polyurethanes. Polymer 47, 319–329. https://doi.org/10.1016/j.polymer.2005.10.107.
Youssef, G., Brinson, J., Whitten, I., 2017. The effect of ultraviolet radiation on the hyperelastic behavior of polyurea. J. Polym. Environ. 0, 1–8. https://doi.org/10.1007/s10924-016-0933-x.
Youssef, G., Gupta, V., 2012a. Dynamic tensile strength of polyurea. J. Mater. Res. 27, 494–499. https://doi.org/10.1557/jmr.2011.405.
Youssef, G., Gupta, V., 2012. Dynamic response of polyurea subjected to nanosecond rise-time stress waves. Mechanics of Time-Dependent Materials 16 (3), 317–328. https://doi.org/10.1007/s11043-011-9164-7.
Youssef, G., Whitten, I., 2017. Dynamic properties of ultraviolet-exposed polyurea. Mech. Time Depend. Mater. 21, 351–363. https://doi.org/10.1007/s11043-016-9333-9.
Youssef, G.H., 2010. Dynamic Properties of Polyurea. University of California, Los Angeles.